

# The intrinsic communication in power systems: a new perspective to understand stability

Yunjie Gu <sup>\* 1,2</sup>, Yitong Li <sup>\* 1</sup>, Timothy C. Green<sup>1</sup>

<sup>1</sup>Imperial College London, London, UK. <sup>2</sup>University of Bath, Bath, UK. <sup>\*</sup>Corresponding Author.

**The large-scale integration of converter-interfaced resources in electrical power systems raises new threats to stability which call for a new theoretic framework for modelling and analysis. In this paper, we present the intrinsic analogy of a power system to a communication system, which is here called power-communication isomorphism. Based on this isomorphism, we revisit power system stability from a communication perspective and thereby establish a theory that unifies the heterogeneous power apparatuses of a power systems and provide a bridge the between the electromagnetic transient (EMT) and phasor analysis frameworks. This theory yields several new insights into power system stability and new possibilities for stabilisation. In particular, we demonstrate that a system of 100% converter-interfaced resources can achieve stable synchronisation in small- and large-signal sense under grid-following control which was commonly considered impossible.**

Driven by the imperative of decarbonisation and clean growth, the primary energy of power systems is transforming from fossil fuels to renewable resources. The change of the primary energy is accompanied by a change of technologies for power generation and conversion. Renewable resources, mainly wind and solar energy, as well as grid-scale battery storage plants, are interfaced to power systems by power electronic converters instead of conventional synchronous generators. The increasing penetration of converter-interfaced resources poses new threats to system stability. Converter-induced oscillations have been reported worldwide, many of which had major consequences. For example, the 2019 power outage in UK was, in part, triggered by a sub-synchronous oscillation of wind turbine converters in Hornsea windfarm according to the report provided by National Grid UK [1]. Some of the new converter-induced oscillation phenomena are beyond the prediction capabilities of state-of-the-art stability models and the underpinning mechanisms are not fully understood and this has drawn international attention.

The stability of a power system is defined as the ability to keep all apparatus in the system synchronised to a single frequency with power flows and voltage profiles throughout the system within some expected range [2], [3]. The classic stability theory for power systems is tailor-made for synchronous generators which are governed by the physical law of the motion of their rotors. However, converters are governed by control algorithms, which gives rise to almost infinite flexibility, and therefore complexity, in converter behaviours [4]. Up to now, the control-defined behaviour of converters are categorised into two classes. The first class, called grid-forming, behaves as a voltage source which synchronises to the grid according to power balancing. The second class, called grid-following, behaves as a current source (or sink) which synchronises to the grid according to voltage signals. This forming-following dichotomy creates a heterogeneous grid that sets a barrier for whole-system analysis [5], [6]. Moreover, the forming-following dichotomy uses only a portion of the controllability of converters and new control algorithms are yet to be explored.

To address this challenge, we looked again at the nature of power systems. We illustrate that there is an intrinsic communication mechanism underlying power systems, which is described

as a power-communication isomorphism. Based on the isomorphism, we developed a theory that creates new insights into power system dynamics and yields new possibilities for stabilisation. We also demonstrate that a power system with nearly 100% converter-interfaced resources under grid-following control can maintain stable synchronisation over various transients, provided that the control parameters are properly designed under the guidance of our new theory. This was commonly considered impossible in state-of-the-art models, and is a surprising and valuable result from the new theory.

## Power-Communication Isomorphism

The concept of power-communication isomorphism is illustrated in Fig. 1. The voltages and currents in a power system are viewed as communication signals carrying both energy and information. The power apparatuses, including generators and converters, serve as modulators in that they create three-phase sinusoidal signals from internal oscillators (or rotors). The amplitude, frequency and phase of an internal oscillator are base-band signals which are shifted to the carrier-band of 50 Hz or 60 Hz via frame transformation or rotation, creating an effect equivalent to amplitude and angle modulation. Mathematically, a three-phase signal is represented as a complex number  $Ae^{j\theta}$ , where  $A$  and  $\theta$  are the amplitude and angle of the signal [7], [8]. The amplitude and angle can be combined into a complex phase defined as  $\vartheta = \ln A + j\theta$ , so the amplitude-angle modulation is jointly expressed as a complex exponential function

$$e^{\vartheta} = Ae^{j\theta} = A(\sin \theta + j \cos \theta) \quad (1)$$

The time-derivative of the  $\vartheta$  is called the complex frequency  $\varpi = \dot{\vartheta} = A^{-1}\dot{A} + j\omega$ , whose real part reflects amplitude variation, and the imaginary part  $\omega = \dot{\theta}$  is the angular frequency.

The modulated signals are propagated over a power network and that network can be viewed as a set of communication channels. The channels include all passive components in the power network, including transmission lines, transformers, series/shunt compensators, harmonic filters, and passive loads. The inner control loops of converters can be represented as equivalent impedances in series or shunt with the sources, and therefore can also be counted among the channels. The active apparatuses, including generators and converters, are defined as nodes that

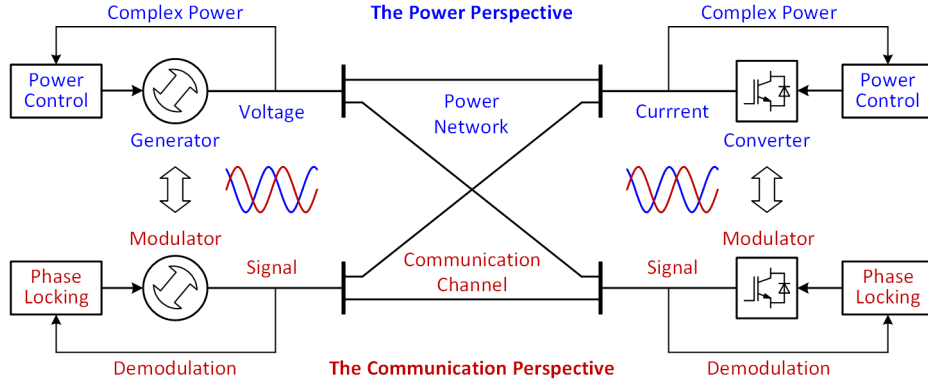


Fig. 1. Illustration of power-communication isomorphism in power systems. The upper part shows a part of system viewed from the perspective of power transfer and the lower part is viewed from the perspective of communication.

interact (communicate) over the channels. There are two types of nodes in a power system. A voltage node applies a voltage source to the network, and represents grid-forming apparatuses, including synchronous generators and grid-forming converters. A current node applies a current source to the network, and represents grid-following converters [4], [9]. From the communication point of view, a voltage node transmits a voltage signal to the network and receives a current signal, and a current node does the opposite. There may be multiple nodes in the network and their signals are received at each node as a single signal by superposition. The complex power seen at a node is defined as [10]

$$S = e^{\vartheta_{tx}} e^{\vartheta_{rx}^*} = A_{tx} A_{rx} e^{j(\theta_{rx} - \theta_{tx})} \quad (2)$$

where  $e^{\vartheta_{tx}}$  is the transmitted signal,  $e^{\vartheta_{rx}}$  is the received signal, and the superscript  $*$  denotes complex conjugation. The direct-quadrature ( $dq$ ) frame transformation of a signal is defined as

$$x_{dq} = e^{\vartheta_{rx}} e^{-j\theta_{tx}} = A_{rx} e^{j(\theta_{rx} - \theta_{tx})} \quad (3)$$

where  $x_{dq}$  is the received signal transformed to the  $dq$  frame oriented to the transmitting angle  $\theta_{tx}$ .  $S$  and  $x_{dq}$  are equivalent (aligned in angle) except for a scaling factor of  $A_{tx}$  in amplitude. The alternating parts of  $e^{\vartheta_{tx}}$  and  $e^{\vartheta_{rx}}$  are cancelled in  $S$  and  $x_{dq}$  which means that the complex power or  $dq$  transformation has a demodulation effect that converts a carrier-band signal back to base-band.

### Unified Synchronisation Principle

Synchronisation is an essential element, and arguably the cornerstone, of power system stability. There are heterogeneous synchronisation schemes co-existing in power systems which present an obstacle to systemic analysis. Voltage nodes use power-based synchronisation via physical or emulated rotors [11], [12], whereas current nodes use signal-based synchronisation via phase-locked loops (PLLs). The theory of power-communication isomorphism illuminates the unified principle underlying the power- and signal-based synchronisation schemes.

The essence of synchronisation is to detect the angle difference between nodes and mitigate the difference via feedback control of the frequency of the oscillators of the nodes in question. In the light of power-communication isomorphism, the demodulated power  $S$  and signal  $x_{dq}$  are natural candidates for

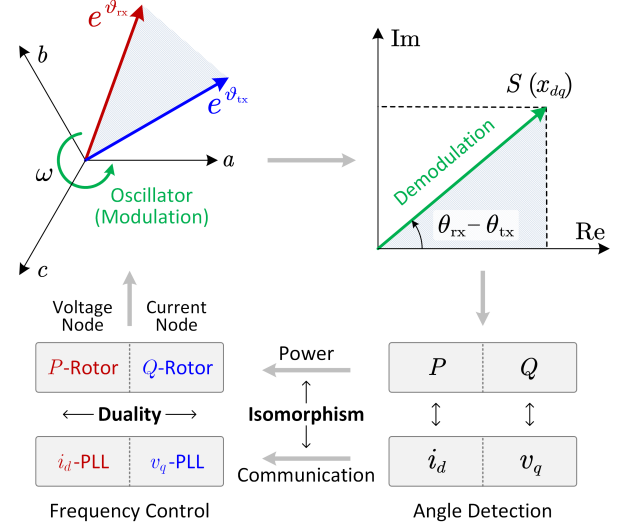


Fig. 2. Unified synchronisation principle in the light of power-communication isomorphism: the equivalence of rotor and PLL, and the duality of voltage and current nodes. We use a prefix to distinguish the conventional rotor and PLL ( $P$ -Rotor,  $v_q$ -PLL) and the ones derived from the isomorphism ( $Q$ -Rotor,  $i_d$ -PLL).

angle detectors. However,  $S$  and  $x_{dq}$  are complex numbers, so their real and imaginary parts are used in practice. For a voltage node, the active power  $P = \text{Re}(S)$  is used as an angle detector; for a current node, the  $q$ -axis voltage  $v_q = \text{Im}(v_{dq})$  is used as an angle detector. From the equivalence of  $S$  and  $x_{dq}$  follows the relationships below

$$P = i_d A_v \propto i_d, \quad Q = v_q A_i \propto v_q \quad (4)$$

where  $i_d = \text{Re}(i_{dq})$  is the  $d$ -axis current,  $Q = \text{Im}(S)$  is the reactive power, and  $A_v$  and  $A_i$  are the amplitudes of voltage and current respectively. This equivalence results in the unified synchronisation principle illustrated in Fig. 3. The rotor of a voltage node is equivalent to a PLL synchronising to the current  $i_d$ , and the PLL of a current node is equivalent to a rotor accelerating/decelerating under reactive power  $Q$ .

The synchronisation of voltage and current nodes has a duality relationship, that is, a voltage node synchronises to a current signal, and a current node synchronises to a voltage signal [13]. When two voltage nodes synchronise, one of the voltage signals

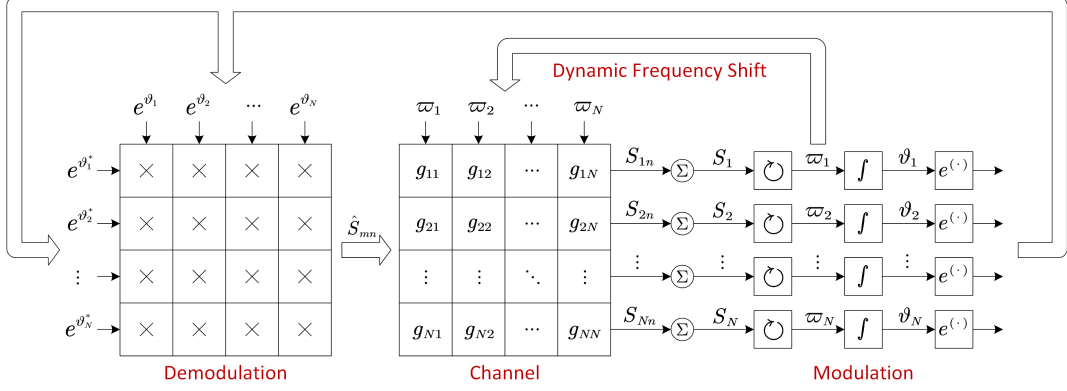


Fig. 3. The overall model of the power-communication isomorphic system considering the dynamic channel gains. Symbols:  $*$  denotes complex conjugation,  $\times$  denotes multiplication,  $\Sigma$  denotes summation,  $\int$  denotes integration, and  $\circlearrowleft$  denotes the oscillator that synthesise the internal complex frequency according to the balancing of the complex power.

is converted to a current signal over the channel, via Norton equivalence. When two current nodes synchronise, one of the current signals is converted to a voltage signal over the channel, via Thévenin equivalence.

Angle detection via  $P$  and  $Q$  can be generalised by introducing a projection angle  $\mu$

$$W = \text{Re}(e^{-j\mu} S) \quad (5)$$

where  $W$  is named *generalised power*, and the associated frequency control is governed by a *generalised rotor*. If  $\mu$  is set to 0 or  $\pi/2$ ,  $W$  reduces to  $P$  or  $Q$  respectively. Setting  $\mu$  to other values creates novel synchronisation schemes that may enhance synchronisation stability, as will be discussed later.

## Channel Dynamics

In a communication system, the dynamics of a communication channel determine the maximum communication rates according to the famous Shannon-Hartley theorem [14]. In this section, we investigate the role of channel dynamics in power systems.

A channel consists of linear circuits and therefore can be represented as a linear transfer function  $G(s)$  in frequency domain. Since the modulation-demodulation has a frequency shifting effect, the equivalent transfer function seen by the base-band signals is shifted to  $G(j\omega_c + s)$  according to Fourier analysis [15]. This frequency shift representation assumes a constant carrier frequency which does not hold for a power system where different nodes may have different instantaneous carrier frequencies that are varying in real-time subject to load balancing. To address this issue, we propose a new time-domain representation for a channel. The time-domain gain of a channel is defined as  $g = e^{\vartheta'}/e^{\vartheta}$  where  $e^{\vartheta}$  and  $e^{\vartheta'}$  are the input and output signals of the channel respectively. The alternating part of  $e^{\vartheta}$  and  $e^{\vartheta'}$  are cancelled in the division so  $g$  is a base-band variable.  $G(s)$  can be decomposed into a series of first-order systems  $G(s) = \sum_k (s - p_k)^{-1} a_k$ , each of which induces a gain  $g_k$ , and the total gain is the sum of all  $g_k$ . We simply investigate one of the first-order systems  $G(s) = (s - p)^{-1} a$  without losing generality, where  $p$  is the pole of  $G(s)$  and  $a$  is the coefficient. The corresponding differential equation for the signal passing the channel is

$$d e^{\vartheta'}/dt = p e^{\vartheta'} + a e^{\vartheta} \quad (6)$$

which yields the differential equation for the channel gain  $g$

$$dg/dt = (p - \varpi)g + a. \quad (7)$$

It is clear that  $g$  depends on  $\varpi$  dynamically, and this effect is named *dynamic frequency shift* as an extension to the (static) frequency shift in Fourier analysis. It is worth noting that the dynamics of  $g$  are non-linear although the channel is linear.

Taking into account the dynamic channel gain, the overall model for the power-communication isomorphic system is illustrated in Fig. 3. For a network with  $N$  nodes, the  $n$ -th node transmits a signal  $e^{\vartheta_n}$  to the network which is demodulated by another node  $m$  to yield  $\hat{S}_{mn} = e^{\vartheta_n} e^{\vartheta_m^*}$ . We put  $\hat{}$  on  $\hat{S}_{mn}$  because it is not physical power as the channel gain is not yet included. Considering the channel gain, the complex power transfer over the channel from the  $n$ -th node to the  $m$ -th node is  $S_{mn} = g_{mn} \hat{S}_{mn}$  where  $g_{mn}$  is the corresponding channel gain. Putting together  $g_{mn}$  for each pair of nodes form a matrix of channel gains which reflects the topology of the network. All traffic in the network shares the channels according to the superposition principle, so the total complex power received at node  $m$  is the summation:  $S_m = \sum_n S_{mn}$ . The total complex power  $S_m$  is fed to the oscillator of the  $m$ -th node. The oscillator governs the complex frequency  $\varpi_m$  which is integrated to the complex angle  $\vartheta_m$ . The signal  $e^{\vartheta_m}$  is modulated from  $\vartheta_m$  and transmitted to channels, and thus closes the loop of modulation-demodulation.

The dynamic frequency shift illuminates interesting properties of base-band signal propagation over a channel. To illustrate this, we find the linearised solution of  $g$  from (7) and put it into  $S_{mn}$

$$\Delta S_{mn} = S_{mn0} (\Delta \vartheta_m^* + F \cdot \Delta \vartheta_n) \quad (8)$$

where the prefix  $\Delta$  and subscript 0 denote the perturbation and equilibrium of a dynamic variable, and  $F$  is a low pass filter

$$F(s) = \frac{j\omega_0 - \lambda}{s + j\omega_0 - \lambda}. \quad (9)$$

It is clear from (8) that a channel induces asymmetry in base-band signal propagation. The angle perturbation  $\Delta \vartheta_m$  at the receiving end  $m$  affects the complex power  $\Delta S_{mn}$  instantaneously, whereas the angle perturbation  $\Delta \vartheta_n$  at the transmitting

end  $n$  passes through a low-pass filter  $F$  before affecting  $\Delta S_{mn}$ . Thus we defined the *channel bandwidth* as

$$\begin{aligned} \omega_b &= \sup |\omega|, \text{ subject to} \\ |F(j\omega)| &> 1/\sqrt{2} \text{ and } |\angle F(j\omega)| < \pi/4. \end{aligned} \quad (10)$$

The channel bandwidth identifies the limit speed of power transfer and angle synchronisation on the channel. The power and angle variations beyond the channel bandwidth are impeded by channels. This has significant impact on power system stability, as we will discuss in the next section. Within the channel bandwidth, the dynamic channel gain  $g$  responds almost instantaneously to  $\varpi$ . In such a case,  $g$  can be approximated by letting  $dg/dt = 0$  in (7) which yields

$$g \approx (\varpi - \lambda)^{-1} \zeta = G(\varpi). \quad (11)$$

The channel dynamics are equivalent to the electromagnetic transients (EMTs) in power systems, and the base-band signals are equivalent to phasors. Therefore, the channel bandwidth determines the boundary where phasor models become inaccurate, and the dynamic channel gain extends the phasor model to include EMT. If the dynamic frequency shift is ignored by assuming  $\varpi \equiv j\omega_0$ ,  $g$  reduces to the conventional phasor model. Thus the dynamic channel gain bridges the gap between EMT and phasor domains and is a useful tool to analyse EMT-phasor interaction.

## Rethinking Power System Stability

The power-communication isomorphism theory provides a new perspective to rethink power system stability. First, the channel bandwidth determines the maximum speed of power transfer and angle synchronisation over the network. The channel bandwidth  $\omega_b$  is determined by the pole  $p$  of the channel. There are four types of channels in a network, namely voltage-voltage, voltage-current, current-voltage, current-current channels. A voltage-voltage channel is the channel between two voltage nodes, and other types are defined similarly. A voltage-voltage channel is generally an inductive transmission line with a very small resistance, so its pole is approximately zero and the corresponding channel bandwidth is  $0.41\omega_0$  ( $\omega_0$  of the power system of 50 or 60 Hz). Other channels where current nodes are associated (i.e., voltage-current, current-voltage, and current-current channels) have a negative-real pole so their channel bandwidths are higher, as marked in Fig. 4 (a). This is because the parallel connected passive loads and the current control loops induce equivalent shunt resistances at the current node which reshapes the channel pole. Due to the relatively low channel bandwidth compared to a current node, a voltage node has a low power control speed, which results in high transient power and energy perturbation, as shown in Fig. 4 (b) and (c). The transient power perturbation is accumulated by the local energy cache (e.g. rotating inertia or dc-link capacitor), and hence a large energy cache is needed for a voltage node to suppress overshoot (e.g. the overshoot of dc-link voltage).

Second, the dynamic frequency shift of channels may induce negative damping and destabilise the system. Combining

the synchronisation principle in (5) with the channel model in Fig. 1, we get the whole-system model:

$$H_m \dot{\omega}_m = W_m^* - \underbrace{\text{Re} \left( e^{-j\mu_m} \sum_n g_{mn} e^{\vartheta_n} e^{\vartheta_m^*} \right)}_{W_m} \quad (12)$$

where  $W_m$  is the generalised power seen at node  $m$ , and  $W_m^*$  is its reference value. The balancing of  $W_m^* - W_m$  governs the frequency  $\omega_m$  of the generalised rotor with  $H_m$  being its generalised inertia<sup>1</sup>. This model is consistent with the phasor model except that the channel gains  $g_{mn}$  are dynamically variable rather than constant, thus the effect of EMTs is included. If the frequency variations are kept within the channel bandwidth, the channel gain is approximated by  $g_{mn} \approx G_{mn}(\varpi_n) = G_{mn}(j\omega_n)$  which is a function of  $\omega_n$ , and so is  $W_m$ . This power-frequency dependency, quantified by  $\partial W_m / \partial \omega_n$ , tends to be negative in many conditions, which induces negative damping and makes the system unstable, as illustrated in Fig. 5. This channel-induced negative damping illuminates the role of EMTs in phasor-domain stability.

Lastly, we demonstrate that a power system with 100% grid-following converters (i.e. no grid forming converters) can be well stabilised in terms of synchronisation, which was generally considered impossible. If sufficient damping is provided in frequency control<sup>2</sup>, the frequency shift effect can be neglected by assuming  $g_{mn} \approx G_{mn}(j\omega_0)$  is constant, and the whole-system model (12) becomes

$$\begin{aligned} H_m \dot{\omega}_m &= W_m^* \\ &- \underbrace{D_m(\omega_m - \omega_0)}_{\text{Generalised Damping}} - \underbrace{\sum_n \Gamma_{mn} \sin(\theta_m - \theta_n + \gamma_{mn})}_{W_m} \end{aligned} \quad (13)$$

where  $D_m$  is the generalised ( $P$ - and  $Q$ -) damping coefficient,  $\Gamma_{mn} = |g_{mn} A_m A_n|$  is the synchronisation coefficient, and  $\gamma_{mn} = \pi/2 + \mu_m - \arg g_{mn}$  is the offset angle. Equation (13) has interesting properties. The synchronisation coefficient  $\Gamma_{mn}$  is symmetric ( $\Gamma_{mn} = \Gamma_{nm}$ ) due to the reciprocity of electrical networks. The offset angle  $\gamma_{mn}$  is dependent on network topology as well as the projection angle  $\mu_m$ . In the following two conditions,  $\gamma_{mn}$  is approximately zero for  $m \neq n$ : (i) synchronisation of grid-forming apparatuses via inductive transmission lines; and (ii) synchronisation of grid-following inverters via shunt resistances (passive loads). In such cases, the synchronisation equation (13) is reduced to a second-order Kuramoto model which has a wide stability region [16]. This implies that grid-following converters may have guaranteed stability that is similar to grid-forming apparatuses.

For cases where grid-forming and grid-following apparatuses co-exist, or where the power network is not purely inductive or resistive,  $\gamma_{mn} \neq 0$ , and the whole-system dynamic behaviour is more complicated. We can use linearisation to evaluate the stability subject to small disturbances. Define  $K_{mn} \triangleq \partial W_m / \partial \theta_n$  and  $[K_H] \triangleq [H]^{-1} [K]$ , where  $[\cdot]$  denotes a matrix or a vector,  $[K]$  is the matrix of  $K_{mn}$ , and  $[H]$  is the diagonal matrix of

<sup>1</sup>In this model we neglect the damping provided by frequency control. The amplitude of all signals are assumed constant so the complex frequency reduces to angular frequency, that is  $\varpi = j\omega$

<sup>2</sup>The damping can be provided explicitly in the form of droop control, or implicitly via proportional control [13].

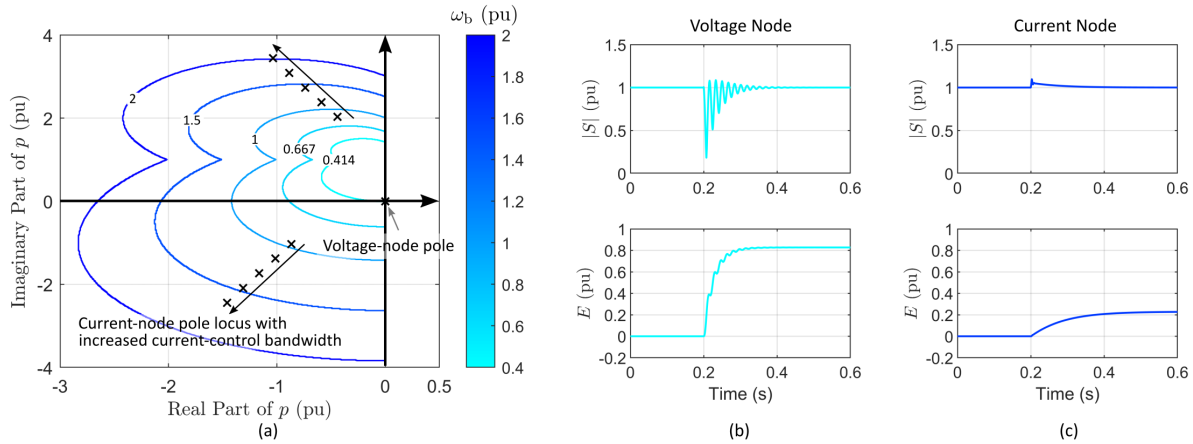


Fig. 4. Channel bandwidth and its impact on transient power. (a) Equi-bandwidth contours on the plane of channel pole indicating that current nodes have higher channel bandwidth  $\omega_b$  than voltage nodes. (b)-(c) Transient power ( $|S|$ ) and the accumulated energy ( $E$ ) at a node subject to a phase jump at the remote end: (b) for a voltage node and (c) for a current node. The relatively low channel bandwidth associated with a voltage node results in high accumulated energy and requires a large energy cache. Some variables in the figure are presented per-unit (pu), and the details of the pu system is explained in Methods.

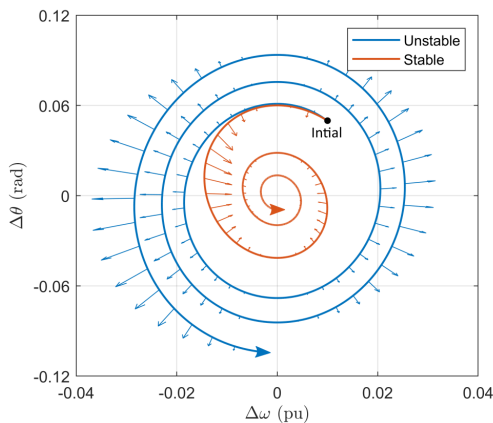


Fig. 5. Dynamic frequency shift may induce negative damping. The negative  $\partial W / \partial \omega$  results in a vector field on the  $\omega$ - $\theta$  phase plane pointing outward (shown as the outward arrow on the blue trajectory), which causes the trajectory to diverge from the equilibrium and makes the system unstable. This problem can be solved by injecting extra positive damping in frequency control, to make the vector field pointing inward (shown as the inward arrow on the amber trajectory).

$H_m$ .  $[K_H]$  is an extension of the synchronising power coefficients in conventional power systems, and therefore can be used as a generalised stability index. The eigenvalue of  $[K_H]$  determines the small-disturbance stability of (13), and the eigenvector determines the modal participation. We define the critical eigenvalue  $\xi_c$  as the non-zero eigenvalue of  $[K_H]$  that has the minimum real part. The system is small-disturbance stable if  $\xi_c$  has a positive real part (see Methods for details).

The offset angle  $\gamma_{mn}$  has significant impacts on whole-system stability. If  $\gamma_{mn}$  is close to zero, (13) is close to the second-order Kuramoto model whose stability region is guaranteed. The offset angle  $\gamma_{mn}$  is affected by the projection angle  $\mu_m$  in angle detection, so we can alter  $\mu_m$  to keep  $\gamma_{mn}$  small. This implies the possibilities of creating new technologies from the power-communication isomorphism theory to enhance stability.

We verified our theoretic findings on the IEEE 68-bus system, and the test results are summarised in Fig. 6. We tested five cases

with different proportions of grid-following converters, subject to small and large disturbances. Tests (a)-(b) contain 100% grid-following converters with passive and active loads, and are stable under both small and large disturbances. We gradually replaced the converters by synchronous generators in tests (c)-(e), and found more complicated stability patterns. These agree well with the prediction of our theory. The critical eigenvalue  $\xi_c$  of  $[K_H]$  provides accurate indication of small-disturbance stability in all cases. We also display in test (c) the participation of each node in the critical eigenvalue, to show how  $[K_H]$  helps to trace the origins of instability.

It is rather surprising to see that a power system with 100% converters (grid-following) is rather stable and re-synchronises rather fast after faults (see Methods for the transient trajectories). It is even more surprising to see that adding one synchronous generator to the all-converter network destabilises the system, which contradicts the conventional observation that synchronous generators are always helpful for grid stability. This phenomenon can be explained by the asymmetry of synchronisation between voltage nodes and current nodes, that is, stability is higher for current nodes following voltage nodes than the opposite (see Methods for details). This raises the important issue about the placement of grid-forming apparatuses in a converter dominated grid. We use two techniques to guide this placement: participation analysis for the critical eigenvalue for small-disturbance stability, and observation of loss of synchronisation via time-domain simulation for large-disturbance analysis. These techniques are effective as verified in tests (c)-(d)-(e), showing succeeding improvements of stability when synchronous generators are placed at the nodes identified most influential (14 and 7).

Grid impedances have significant impacts on system stability. We shaded the grid map in Fig. 6 by the magnitude of the Thevenin impedance seen at each node. It is clear that small impedances tend to enhance stability. The grid impedances are resistive for case (a), capacitive-inductive (i.e., some nodes see capacitive Thevenin impedances, and others see inductive) for case (b), and inductive for case (c)-(e), because the impedances are dominated by passive loads, shunt capacitances, and trans-

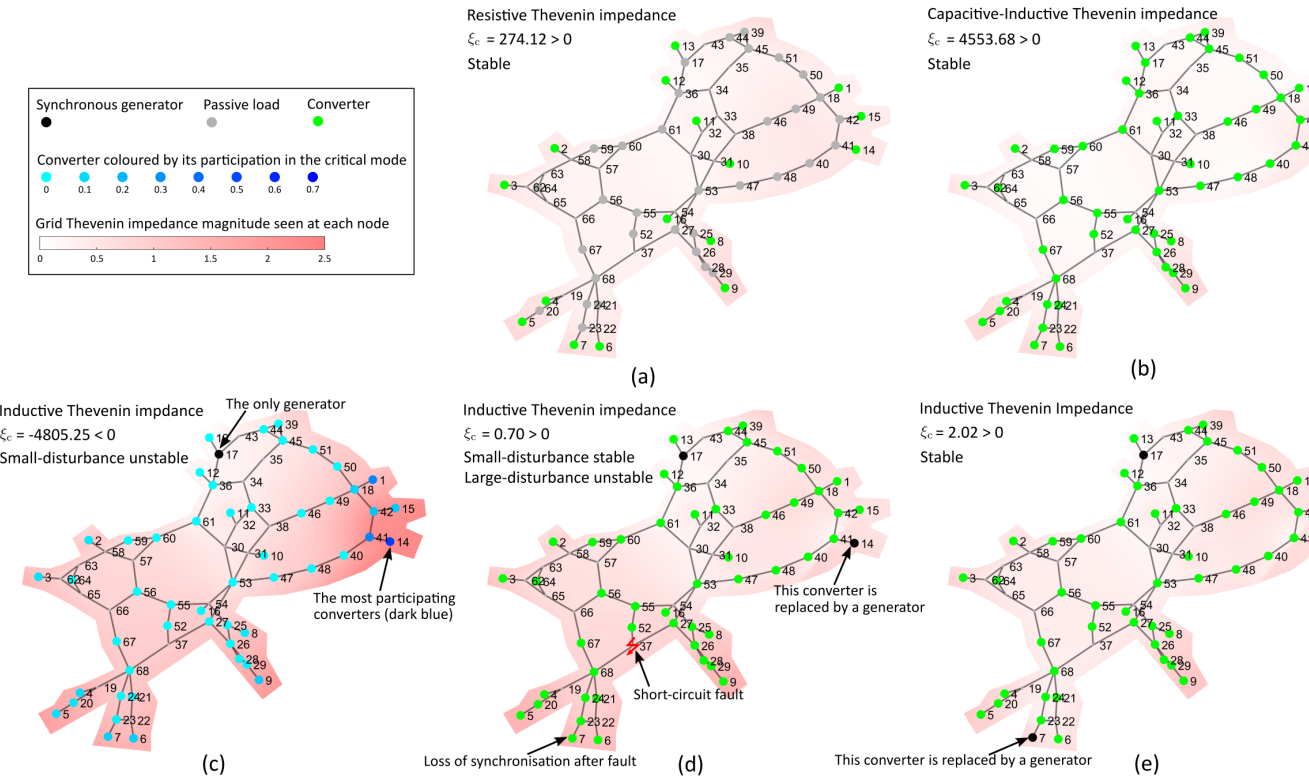


Fig. 6. Summary of test results on the IEEE 68-bus system with varying numbers of grid-following converters (green dots), synchronous generators (black dots) and passive loads (grey dots). Heat-map in shades of red indicates impedance magnitude seen at each node. The small-disturbance and large-disturbance stability of the tested system is marked via texts on the map, and the detailed transient responses are shown in methods. (a) 17 converters, 0 synchronous generators, with passive loads. (b) Converters at all 68 busses with active loads. (c) 1 synchronous generator (at node 17). (d) 2 synchronous generators (at nodes 14,17). (e) 3 synchronous generators (at nodes 7,14,17).

mission lines respectively. These impedance characteristics play important roles in the stability of the corresponding cases, as explained in Methods.

It needs to be acknowledged that we have assumed the amplitudes of currents are constant for grid-following converters in the dynamic model in (13). This is not the case in practice since the currents are changed according to the desired power injection or consumption. However, it is reasonable to assume constant currents in faults because the current controllers of converters are saturated to the rated currents for self-protection. Under normal condition, the currents can be adjusted by slow secondary control which have separated timescales to the angle-synchronisation so the dynamic interaction between amplitudes and angles are assumed negligible.

## Discussions

The power-communication isomorphism theory reveals the intrinsic analogy of power systems and communication systems. This analogy (isomorphism) sheds light on the stability of power systems from a communication perspective. The power-based and signal-based synchronisation schemes are unified into a common principle. The dynamic channel gain bridges the gap between EMT and phasor domains. It is proved that the channel bandwidth determines the limit speed of power transfer and angle synchronisation, and the channel-frequency dependency induces negative damping in whole-system stability. These new findings provide new guidelines on whole-system stability, including the configuration of local energy caches and damping

controls, and new technologies for stability enhancement. We also demonstrate that a power system with 100% grid-following converters can be well stabilised, which was believed impossible. All of the major findings are verified on the modified IEEE 68-bus test system.

## Methods

**Channel Bandwidth.** The channel bandwidth equations (8)-(9) are obtained as follows. Applying angle perturbations at both ends of the channel  $g_{mn}$ , the corresponding complex power perturbation is

$$\Delta S_{mn} = S_{mn0}(\Delta\vartheta_m^* + \Delta\vartheta_n + g_{mn0}^{-1}\Delta g_{mn}). \quad (14)$$

Linearising the channel gain equation (7) yields

$$d\Delta g/dt = (\lambda - \varpi_0)\Delta g - g_0\Delta\varpi \quad (15)$$

from which we get the transfer function from  $\Delta\varpi$  to  $\Delta g$

$$\Delta g(s) = -\frac{g_0}{s + \varpi_0 - \lambda}\Delta\varpi(s). \quad (16)$$

Therefore,

$$g_{mn0}^{-1}\Delta g_{mn}(s) = \frac{-\Delta\varpi_n(s)}{s + \varpi_0 - \lambda} = \frac{-s\Delta\vartheta_n(s)}{s + \varpi_0 - \lambda}. \quad (17)$$

Putting this into (14) and noting that  $\varpi_0 = j\omega_0$  (since the signal amplitude is constant in steady-state), we get the equations (8)-(9).

TABLE I  
CHANNEL GAINS AND THE ASSOCIATED SYNCHRONISATION PARAMETERS FOR THE CASES IN FIG. 7

Case	$g_{11}$	$g_{22}$	$g_{12}$	$g_{21}$	$\mu_1$	$\mu_2$	$\Gamma_{mn}$	$\gamma_{11}$	$\gamma_{12}$	$\gamma_{21}$	$\gamma_{22}$	$\Gamma_\delta$	$\gamma_\delta$	$W_\delta^*$
(a)	$e^{-j\varphi}/Z$	$e^{j(\pi-\varphi)}/Z$	0	0	$V^2/Z$		$\frac{\pi}{2} + \varphi$	$\varphi - \frac{\pi}{2}$	$\varphi - \frac{\pi}{2}$	$\frac{\pi}{2} + \varphi$		$\sin \varphi V^2/Z$	0	$P^*$
(b)		$Ze^{j\varphi}$	$-\frac{\pi}{2}$	$-\frac{\pi}{2}$	$I^2 Z$		$-\varphi$	$-\varphi$	$-\varphi$	$-\varphi$		$\cos \varphi I^2 Z$	0	$Q^*$
(c)		$Ze^{j\varphi}$	$-\frac{\pi}{2}$	$\frac{\pi}{2}$	$I^2 Z$		$-\varphi$	$-\varphi$	$\pi - \varphi$	$\pi - \varphi$		$\sin \varphi I^2 Z$	$-\frac{\pi}{2}$	$\Gamma_\delta - Q^*$
(d)	$jX$	$\frac{-j}{X}$	1	-1	$-\frac{\pi}{2}$	0	See Note	$-\frac{\pi}{2}$	0	$-\frac{\pi}{2}$	$\pi$			Depends on $H_1$ and $H_2$

Note: For case (a),  $W_1^* = -W_2^* = P^*$ . For case (b)-(c),  $W_1^* = -W_2^* = Q^*$ . For case (d),  $\Gamma_{11} = I^2 X$ ,  $\Gamma_{12} = V^2/X$ , and  $\Gamma_{12} = \Gamma_{21} = VI$ .

**Channel Gains and Topology.** The channel gains  $g_{mn}$  between each pair of nodes form a matrix  $[g]$  (we use  $[\cdot]$  to denote a matrix or vector). The channel gain matrix  $[g]$  reflects the communication topology of the network. On the other hand, the nodal admittance matrix  $[Y]$  defines the power (physical) topology of the network. We show how the communication and power topology are related. Suppose that the voltage nodes in the network are numbered by  $\{1, 2, \dots, N_v\}$  and current nodes by  $\{N_v + 1, N_v + 2, \dots, N_v + N_i\}$ , where  $N_v$  and  $N_i$  are the total number of voltage and current nodes respectively and  $N_v + N_i = N$ . We partition  $[Y]$  at the  $N_v$ -th row and  $N_v$ -th column:

$$[Y] = \begin{bmatrix} [Y_{vv}] & [Y_{vi}] \\ [Y_{iv}] & [Y_{ii}] \end{bmatrix} \quad (18)$$

and we have

$$\begin{aligned} [i_v] &= [Y_{vv}][v_v] + [Y_{vi}][v_i] \\ [i_i] &= [Y_{iv}][v_v] + [Y_{ii}][v_i] \end{aligned} \quad (19)$$

where  $[v_v]$  and  $[v_i]$  are vectors representing the voltages at the voltage and current nodes respectively, and  $[i_v]$  and  $[i_i]$  are the corresponding current vectors. From the communication perspective,  $[v_v]$  and  $[i_i]$  are transmitted by nodes, and  $[i_v]$  and  $[v_i]$  are received from the network. Thus we rearrange (19) to show the mapping from  $[v_v, i_i]$  to  $[i_v, v_i]$

$$\begin{aligned} [i_v] &= ([Y_{vv}] - [Y_{vi}][Y_{ii}]^{-1}[Y_{iv}])[v_v] + [Y_{vi}][Y_{ii}]^{-1}[i_i] \\ [v_i] &= -[Y_{ii}]^{-1}[Y_{iv}][v_v] + [Y_{ii}]^{-1}[i_i] \end{aligned} \quad (20)$$

from which follows

$$[g] = \begin{bmatrix} [Y_{vv}] - [Y_{vi}][Y_{ii}]^{-1}[Y_{iv}] & [Y_{vi}][Y_{ii}]^{-1} \\ -[Y_{ii}]^{-1}[Y_{iv}] & [Y_{ii}]^{-1} \end{bmatrix}. \quad (21)$$

If the network only contains voltage nodes,  $[g] = [Y]$ , indicating that the communication and power topology are identical. Otherwise, the power topology  $[Y]$  is twisted in the communication topology  $[g]$  due to the interaction of current and voltage nodes. Therefore, the type of nodes essentially affects the network topology.

**Impedance and Stability.** The characteristics of grid impedance have a significant impact on system stability. We illustrated this impact via a simple two-node system:

$$\begin{aligned} H\dot{\omega}_1 &= W_1^* - \Gamma_{11} \sin(\gamma_{11}) - \Gamma_{12} \sin(\theta_1 - \theta_2 + \gamma_{12}) \\ H\dot{\omega}_2 &= W_2^* - \Gamma_{22} \sin(\gamma_{22}) - \Gamma_{21} \sin(\theta_2 - \theta_1 + \gamma_{21}) \end{aligned} \quad (22)$$

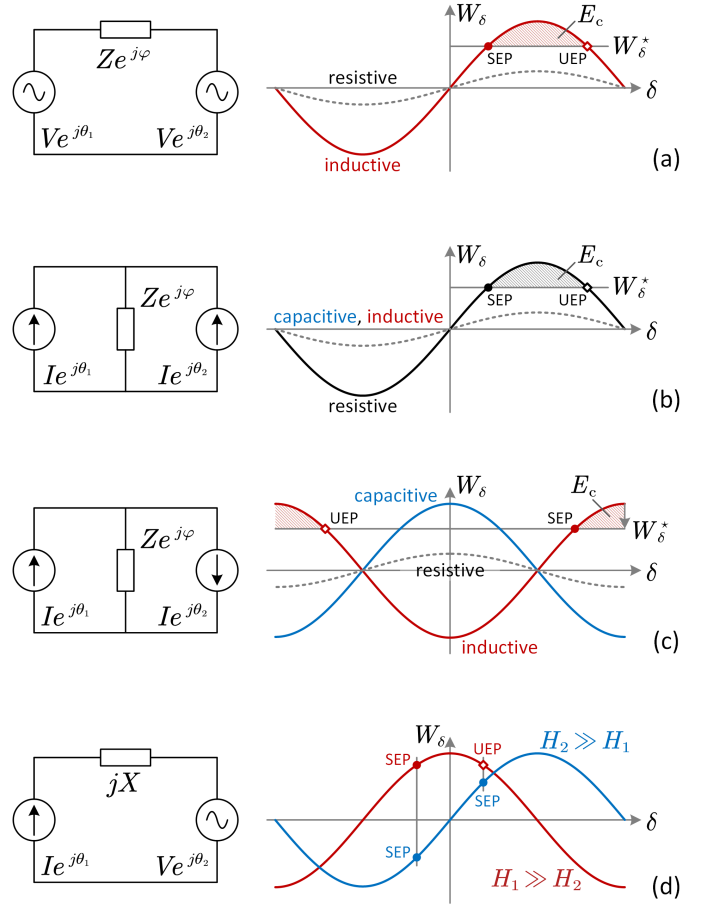


Fig. 7. The impact of channel gain on the synchronisation between different types of nodes. (a) Synchronisation of two grid-forming apparatuses. (b) Synchronisation of two grid-following converters (sources). (c) Synchronisation of a grid-following source with a grid-following load (active load). (d) Asymmetry in the synchronisation between current and voltage nodes.

where we assume the generalised inertias of the two nodes are identical and the dampings are neglected. The two-node interaction can be investigated by taking the difference of the two equations in (22)

$$H_\delta \dot{\omega}_\delta = W_\delta^* - \underbrace{\Gamma_\delta \sin(\delta + \gamma_\delta)}_{W_\delta} \quad (23)$$

where

$$\begin{aligned}\delta &= \theta_1 - \theta_2, \quad \omega_\delta = \omega_1 - \omega_2 = \dot{\delta}, \quad H_\delta = H/2, \\ W_\delta^* &= \frac{1}{2}(W_1^* - W_2^* + \Gamma_{22} \sin \gamma_{22} - \Gamma_{11} \sin \gamma_{11}), \\ \Gamma_\delta &= \Gamma_{12} \cos \frac{1}{2}(\gamma_{12} + \gamma_{21}), \quad \gamma_\delta = \frac{1}{2}(\gamma_{12} - \gamma_{21}),\end{aligned}\quad (24)$$

and we make use of the fact that  $\Gamma_{12} = \Gamma_{21}$ . We use (23) to examine the three cases in Fig. 7 (a)-(c), where two nodes are connected via series or shunt impedance  $Ze^{j\varphi}$ . The channel gains and the associated synchronisation parameters for the three cases are listed in Table I. The  $W_\delta$  is plotted against  $\delta$  in Fig. 7 for different impedance angle  $\varphi$ . The intersection of  $W_\delta$  with  $W_\delta^*$  is the equilibrium point of synchronisation. Since  $W_\delta$  is a sinusoidal function of  $\delta$ , there might be two intersection points for  $\delta \in (-\pi, \pi]$ . The intersection point at the rising edge of  $W_\delta$  is the stable equilibrium point (SEP), and the one at the falling edge of  $W_\delta$  is the unstable equilibrium point (UEP). The area encircled by  $W_\delta$  and  $W_\delta^*$  between the SEP and UEP is called the critical energy  $E_c$ , which defines the maximum transient energy that can be injected into the system without affecting synchronisation stability [17].  $E_c$  is a reflection of the transient stability margin and is dependent upon the interconnection impedance  $Ze^{j\varphi}$  between the two nodes. For case (a) in Fig. 7,  $E_c$  is highest if  $Ze^{j\varphi}$  is inductive, and  $E_c$  reduces if  $Ze^{j\varphi}$  changes from inductive to resistive ( $\varphi$  reduces from  $\pi/2$  to 0), until there are no longer an SEP and the two nodes lose synchronisability at all. Fig. 7 (b) is similar to Fig. 7 (a) except that a resistive  $Ze^{j\varphi}$  offers the highest  $E_c$ , and an inductive or capacitive  $Ze^{j\varphi}$  reduces synchronisation stability. These two cases shows that different impedance angles (representing channel phase shift) are preferred for the synchronisation of grid-forming and grid-following apparatuses. The synchronisation of grid-following converters is sensitive to the direction of power flow, as is clear to see from Fig. 7 (b)-(c). In Fig. 7 (c), one of the grid-following converters is changed from a source to a load, and the synchronisation pattern is significantly different, compared to Fig. 7 (b) where both converters are sources. The source-load synchronisation in Fig. 7 (c) prefers either an inductive or capacitive  $Ze^{j\varphi}$ , in contrast to the preference of resistive  $Ze^{j\varphi}$  in Fig. 7 (b).

**Asymmetry of Voltage and Current Nodes.** Hybrid connection of voltage and current nodes induces asymmetry which hampers stability. We use the case in Fig. 7 (d) to illustrate this, where a current node is connected to a voltage node via an inductive impedance  $jX$ . The corresponding channel gains and synchronisation parameters are given in Table I, and the system equations are

$$\begin{aligned}H_1 \dot{\omega}_1 &= W_1^* + I^2 X - VI \sin \delta \\ H_2 \dot{\omega}_2 &= W_2^* + VI \cos \delta\end{aligned}\quad (25)$$

where  $\delta = \theta_1 - \theta_2$ . The dynamics governed by (25) are dependent upon the ratio of  $H_1/H_2$ . If  $H_2 \gg H_1$ , the voltage node has very high inertia so the current node follows the voltage node. In such a case,  $\dot{\omega}_2 \approx 0$  and  $\dot{\omega}_\delta = \dot{\omega}_1 - \dot{\omega}_2 \approx \dot{\omega}_1$ , so

$$H_1 \dot{\omega}_\delta = \underbrace{W_1^* + I^2 X}_{W_\delta^*} - \underbrace{VI \sin \delta}_{W_\delta} \quad (26)$$

If  $H_1 \gg H_2$ , the voltage node follows the current node and the equation becomes

$$H_2 \dot{\omega}_\delta = \underbrace{-W_2^*}_{W_\delta^*} - \underbrace{VI \cos \delta}_{W_\delta}. \quad (27)$$

The equations (26) and (27) represent very different synchronisation dynamics as are illustrated in Fig. 7 (d), which reflects asymmetry of synchronisation. Equation (26) corresponds to the blue curve and (27) corresponds to the red curve in Fig. 7 (d). Since the SEP of synchronisation must be on the rising edge of the  $W_\delta$  curve, the two curves in Fig. 7 (d) have different stability ranges:  $\delta \in (-\pi/2, \pi/2)$  for  $H_2 \gg H_1$ , and  $\delta \in (-\pi, 0)$  for  $H_1 \gg H_2$ . In practice,  $\delta$  operates within  $(-\pi/2, \pi/2)$  which coincides with the stability range of  $H_2 \gg H_1$ , but  $H_1 \gg H_2$  may become unstable for  $\delta \in (0, \pi/2)$ . As a result,  $H_2 \gg H_1$  (current nodes following voltage nodes) is preferred over  $H_1 \gg H_2$  (voltage nodes following current nodes). The asymmetry of voltage-current synchronisation helps to explain why test (c) is unstable but tests (d)-(e) gradually becomes stable in Fig. 6. The addition of further synchronous generators in tests (d)-(e) increase the total inertia of voltage nodes and thus enhances current-to-voltage synchronisation.

**Small-Disturbance Stability.** Now we show why the small-disturbance stability of the whole system is determined by the eigenvalues of  $[K_H]$ . Linearising (13) yields

$$[\ddot{\theta}] = -[H]^{-1}[D][\dot{\theta}] - [K_H][\Delta\theta] \quad (28)$$

where we make use of the fact that  $[\Delta\omega] = [\dot{\theta}]$ . The generalised inertia and damping are usually proportional, so we have  $[H]^{-1}[D] = \sigma[I]$  where  $[I]$  is a unit matrix and  $\sigma = D_m/H_m$ . Suppose that  $[K_H]$  has not repeated eigenvalues, it can be diagonalised by similarity transformation  $[K_H] = [\Phi][\Xi][\Phi]^{-1}$  where  $[\Xi]$  is a diagonal matrix containing the eigenvalues of  $[K_H]$ , and  $[\Phi]$  contains the corresponding eigenvectors. Define the coordinate transformation  $[\Phi]^{-1}[\Delta\theta] = [z]$ , and transform (28) to the  $z$  coordinate

$$\ddot{z} = -\sigma \dot{z} - [\Xi][z]. \quad (29)$$

Since  $[\Xi]$  is diagonal, (29) reduces to a series of decoupled second order systems

$$\ddot{z}_m = -\sigma \dot{z}_m - \xi_m z_m \quad (30)$$

where  $m \in \{1, 2, \dots, N\}$ ,  $N$  is the total number of nodes, and  $\xi_m$  is the  $m$ -th eigenvalue of  $K_H$ . The system (30) is stable if and only if its characteristic equation  $s^2 + \sigma s + \xi_m = 0$  only has solutions in the left open half complex plane. We traverse  $s$  in the unstable right half plane to get the forbidden region of  $\xi_m$ , and the stable region is its complement

$$\text{Stable Region: } \{\xi_m \mid \text{Re } \xi_m > \sigma^{-2}(\text{Im } \xi_m)^2\}. \quad (31)$$

If sufficient damping is provided in synchronisation control,  $\sigma$  is large enough to render  $\sigma^{-2}(\text{Im } \xi_m)^2$  very small, and the stability region is approximated by

$$\text{Stable Region: } \{\xi_m \mid \text{Re } \xi_m > 0\}. \quad (32)$$

All  $\xi_m$  must be within the stable region to ensure the synchronisation stability of the power system, with the only exception

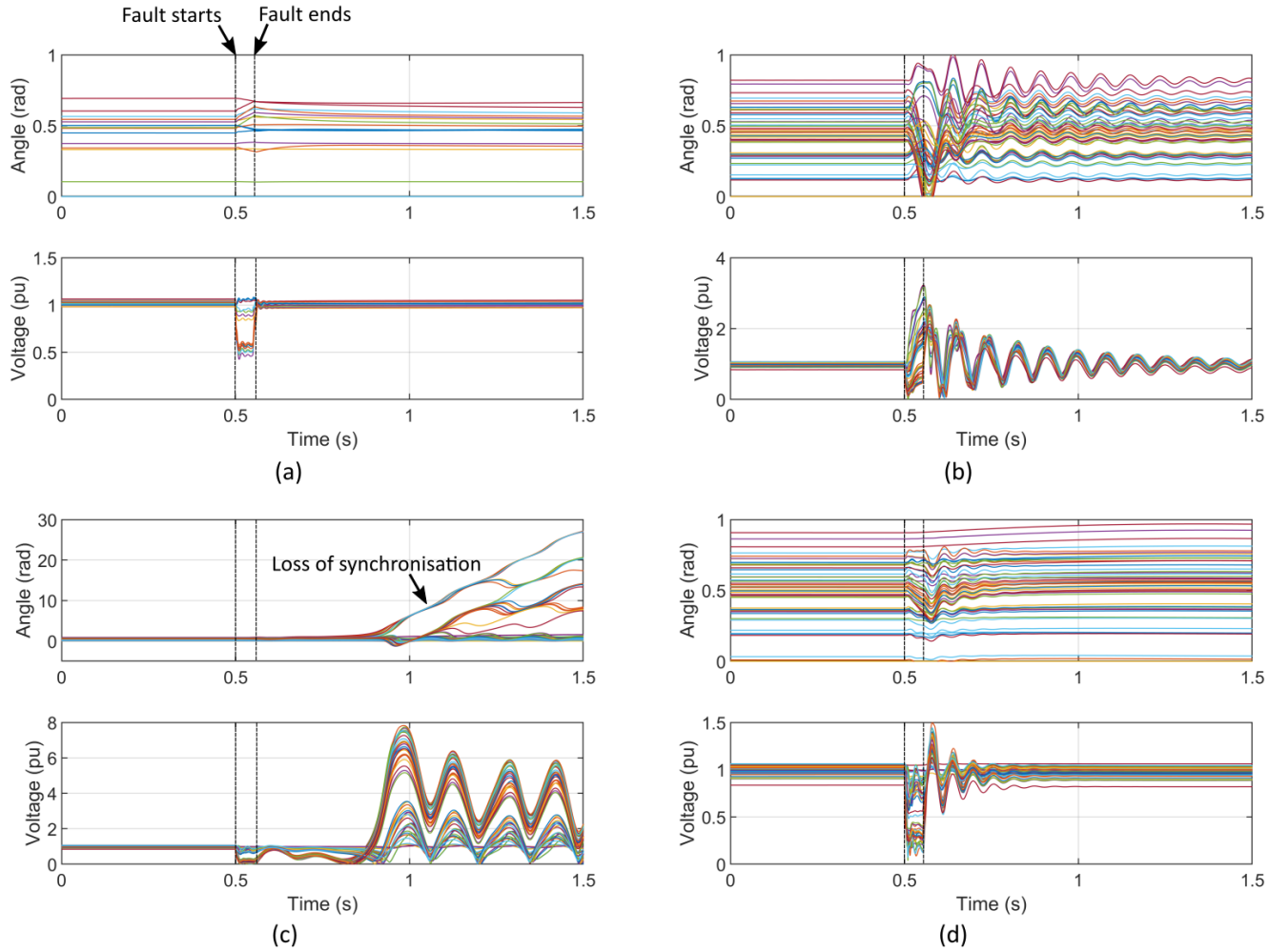


Fig. 8. Time-domain transient trajectories of the modified IEEE 68-bus system under a short-circuit fault, which occurs at bus 37 at 0.5 s and is cleared after 3 fundamental cycles, i.e., at 0.55 s. (a) 100% converters (grid-following) with passive loads. (b) 100% converters with active loads. (c) Two synchronous generators (at node 14,17). (d) Three synchronous generators (at node 7,14,17). The results in (a)-(d) corresponds to tests (a),(b),(d) and (e) in Fig. 6. The simulation result for test (c) is not stable around the equilibrium and is therefore not presented.

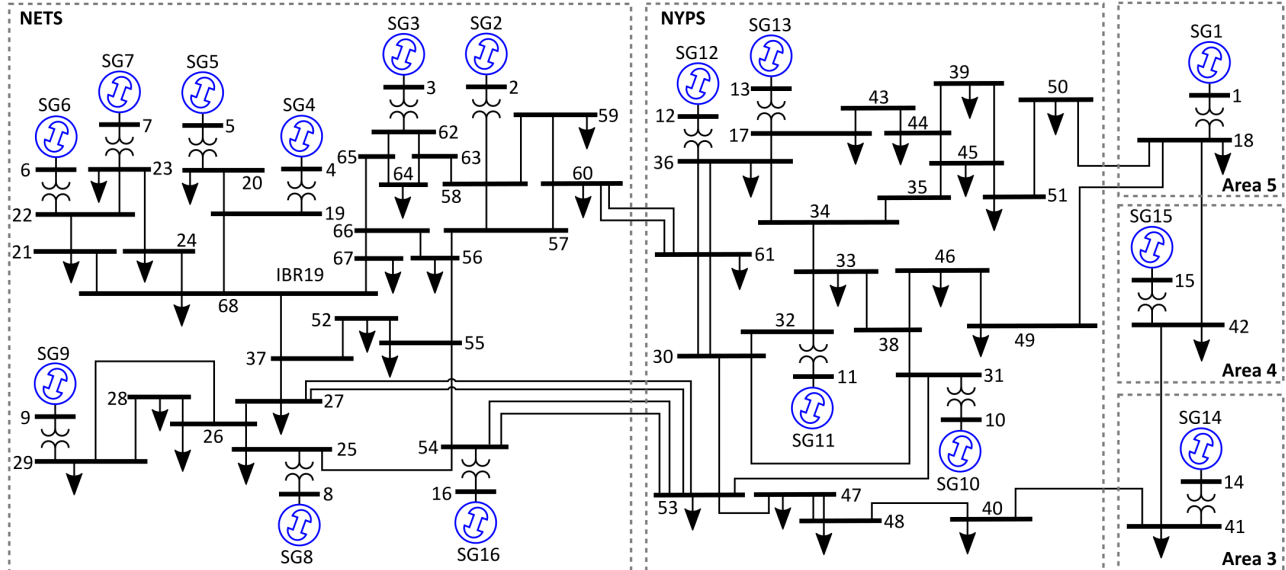


Fig. 9. Layout of the standard IEEE 68-bus NETS-NYPS power system. The system is modified by replacing synchronous generators with converters, and replacing passive loads with active loads in some cases. The configuration transmission lines, shunt commentator, and power flows are not changed.

being the one that equals zero, which represents the collective spinning of the entire power system. Therefore we define the critical eigenvalue  $\xi_c$  as the non-zero  $\xi_m$  (eigenvalue of  $[K_H]$ ) that has the minimum real part.

**Test Configurations and Results.** The tested power system is built by modifying the standard IEEE 68-bus power system in Fig. 9. The IEEE 68-bus power system is a real-world system containing the interconnected New England Test System (NETS) and New York Power System (NYPS) [18]. This system has rich features and therefore is widely used in stability analysis. The buses in Fig. 9 are numbered in the same order as are the nodes in Fig. 6, and we use the terms “bus” and “node” interchangeably.

We replace the synchronous generators in the IEEE 68-bus system by grid-following converters to create a full converter system for test (a) in Fig. 6. The grid-following converters operate with fixed reference values for real and reactive power which have been chosen to achieve the desired steady-state operating point in terms of bus voltages and system frequency. We further replace the passive loads (resistive) by active loads (that is, loads that are interfaced by grid-following converters) for test (b). Tests (c)-(e) are configured by using synchronous generators to replace converters at nodes 17, 14 and 7 in succession.

Numerical simulation is conducted in Matlab/Simulink to generate the time-domain trajectories in Fig. 8. The grid-following converters used the full-order average model with an inner current loop, PLL, and harmonic filter. The current reference for the inner current loop is set to a constant value and no voltage saturation is implemented. The fourth-order model is used for synchronous generators which is a minimum model that preserves both electrical and mechanical dynamics.

All variables in this paper are presented in generator convention (also known as source convention, active sign convention), which defines the electric power flowing out of an apparatus as positive. Some variables are presented in per-unit (pu), which expresses a variable as normalised to a base value. The base values used are listed here: base frequency 60 Hz, base power 100 MVA, and base energy 1.67 MJ; the base energy equals the base power divided by the base frequency for consistency. The details of the the simulation models, code scripts, and system parameters used in this paper, are all available online at [19].

Finally, we present some interpretations of the simulation results in Fig. 8. The recovery from faults in Fig. 8 (a) [test (a) in Fig. 6] is very fast and this reflects the extended synchronisation stability of grid-following converters with passive loads. Fig. 8 (b) [test (b) in Fig. 6] shows angle swing after faults that converge back to the equilibrium, which is similar to the angle swing of synchronous generators but is much faster, since the high channel bandwidth enables faster synchronisation. Excessive voltage overshoots are observed in this test, which is because the converters in our model do not implement voltage saturation. The voltage saturation may induce control logic switching and result in more complicated dynamics. Fig. 8 (c) [test (d) in Fig. 6] shows loss of synchronisation after the fault from which we identified the most vulnerable node which guide the placement of grid-forming apparatuses. Fig. 8 (d) [test (e) in Fig. 6] is similar to Fig. 8 (b) but the voltage overshoot is much reduced because the additional synchronous generator

clamps grid voltages and reduces the grid Thevenin impedances.

## Authors Contributions

Y. Gu proposed the power-communication isomorphism theory. Y. Li applied the theory to power system stability analysis, and implemented the simulations. T. C. Green interpreted the results of the analysis and simulation. Y. Gu, Y. Li, and T. C. Green wrote the paper.

## REFERENCES

- [1] J. Bialek, “What does the GB power outage on 9 august 2019 tell us about the current state of decarbonised power systems?” *Energy Policy*, vol. 146, p. 111821, 2020.
- [2] P. Kundur, *Power system stability and control*. McGraw-hill New York, 1994, vol. 7.
- [3] P. Kundur *et al.*, “Definition and classification of power system stability ieee/cigre joint task force on stability terms and definitions,” *IEEE Trans. Power Syst.*, vol. 19, no. 3, pp. 1387–1401, 2004.
- [4] J. Rocabert, A. Luna, F. Blaabjerg, and P. Rodríguez, “Control of power converters in AC microgrids,” *IEEE Trans. Power Electron.*, vol. 27, no. 11, pp. 4734–4749, Nov. 2012.
- [5] System Operability Framework, “Performance of Phase-locked Loop based converters,” National Grid, Tech. Rep., 2018.
- [6] G. Wu, B. Zhao, X. Zhang, S. Wang, A. Egea-Álvarez, Y. Sun, Y. Li, D. Guo, and X. Zhou, “Impact of non-minimum-phase zeros on the weak-grid-tied VSC,” *IEEE Transactions on Sustainable Energy*, vol. 12, no. 2, pp. 1115–1126, 2020.
- [7] K. W. Martin, “Complex signal processing is not complex,” *IEEE Transactions on Circuits and Systems I: Regular Papers*, vol. 51, no. 9, pp. 1823–1836, 2004.
- [8] F. Briz, M. W. Degner, and R. D. Lorenz, “Analysis and design of current regulators using complex vectors,” *IEEE Transactions on Industry Applications*, vol. 36, no. 3, pp. 817–825, 2000.
- [9] D. Pattabiraman, R. Lasseter, and T. Jahns, “Comparison of grid following and grid forming control for a high inverter penetration power system,” in *2018 IEEE Power & Energy Society General Meeting (PESGM)*. IEEE, 2018, pp. 1–5.
- [10] L. S. Czarnecki, “On some misinterpretations of the instantaneous reactive power pq theory,” *IEEE transactions on power electronics*, vol. 19, no. 3, pp. 828–836, 2004.
- [11] L. Zhang, L. Harnefors, and H.-P. Nee, “Power-synchronization control of grid-connected voltage-source converters,” *IEEE Transactions on Power systems*, vol. 25, no. 2, pp. 809–820, 2009.
- [12] S. D’Arco and J. A. Suul, “Equivalence of Virtual Synchronous Machines and Frequency-Droops for Converter-Based MicroGrids,” *IEEE Transactions on Smart Grid*, vol. 5, no. 1, pp. 394–395, Jan 2014.
- [13] Y. Li, Y. Gu, and T. C. Green, “Revisiting grid-forming and grid-following inverters: A duality theory,” *IEEE Transactions on Power Systems*, 2022.
- [14] W. K. Chen, *The electrical engineering handbook*. Elsevier, 2004.
- [15] A. Oppenheim, A. S. Willsky, and I. Young, “Signals and systems,” *Prentice-Hall, Englewood Cliffs, New Jersey*, vol. 19, pp. 146–153, 1983.
- [16] J. Peng, “Synchronization in the second-order kuramoto model,” 2015.
- [17] H.-D. Chiang and J. S. Thorp, “Stability regions of nonlinear dynamical systems: A constructive methodology,” *IEEE Transactions on Automatic Control*, vol. 34, no. 12, pp. 1229–1241, 1989.
- [18] C. Canizares, T. Fernandes, E. Geraldi, L. Gerin-Lajoie, M. Gibbard, I. Hiskens, J. Kersulis, R. Kuiva, L. Lima, F. DeMarco *et al.*, “Benchmark models for the analysis and control of small-signal oscillatory dynamics in power systems,” *IEEE Transactions on Power Systems*, vol. 32, no. 1, pp. 715–722, 2016.
- [19] “Future Power Networks.” [Online]. Available: <https://github.com/Future-Power-Networks/Publications>